

A Comparative Study of Fitting Techniques

J. Morales, E. Medina, J. Mahseredjian, A. Ramirez, K. Sheshyekani

Abstract--This paper presents a theoretical review and comparison between Vector fitting, Matrix-Pencil-Method and Loewner Matrix techniques for the fitting of frequency-domain functions. Firstly, the theoretical basis of each technique is briefly reviewed. Subsequently, their computational performances are compared through different case studies. As for the Loewner Matrix method, a novel implementation is proposed for a fair comparison with the other two techniques. This novel implementation has some advantages over the traditional one. Global remarks and recommendations are given to take advantage of the capabilities that each technique exhibits.

Keywords: Loewner Matrix, Matrix Pencil Method, Singular Value Decomposition, Vector Fitting.

I. INTRODUCTION

RATIONAL fitting represents a powerful modelling strategy that provides accurate frequency-dependent representation of network elements. Among the applications of rational fitting are the modelling of transmission lines [1], transformers [2] and Frequency-Dependent Network Equivalents (FDNE) [3].

The Vector Fitting (VF) technique [3-5] has been widely used among the power systems community, although, alternative techniques such as Matrix-Pencil-Method (MPM) [6, 7] and Loewner Matrix (LM) [8-10] have also been proposed. These alternative techniques are said to have unique advantages, such as being non-iterative, allowing easy determination of model order, no specification of initial poles and reliable performance for handling noisy samples.

The aim of this paper is to achieve a comprehensive comparison of the abovementioned techniques. The study of the passivity of rational models is beyond the scope of the paper since none of the studied techniques can guarantee this requirement. Then, the paper focuses on the fitting accuracy of the studied fitting techniques.

The rest of the paper is constituted as follows. A brief theoretical review on VF, MPM and LM techniques is presented in Section II. Their performances are assessed through different case studies in Section III. A discussion and summary about the obtained results is presented in Section IV.

This work was supported by NSERC, Hydro-Québec, RTE, EDF and OPAL-RT as part of the industrial chair "Multi time-frame simulation of transients for large scale power systems."

J. Morales, J. Mahseredjian and K. Sheshyekani are with the Power Systems Department, Polytechnique de Montreal, C.P. 6079, Montréal (Québec) H3C 3A7, Canada (e-mail: jesus.morales-rodriguez@polymtl.ca, jean.mahseredjian@polymtl.ca, keyhan.sheshyekani@polymtl.ca).

A. Ramirez and E. Medina are with CINVESTAV-Guadalajara, Guadalajara 45019, Mexico (e-mail: abner.ramirez@cts-design.com, eymedina@gdl.cinvestav.mx).

Paper submitted to the International Conference on Power Systems Transients (IPST2019) in Perpignan, France June 17-20, 2019.

II. REVIEW OF FITTING TECHNIQUES

The general purpose of fitting techniques is to approximate a numerical frequency-domain function $f(s = j\omega)$ as a sum of partial fractions as shown in (1).

$$f(s) \approx \sum_{k=1}^N \frac{c_k}{s - a_k} + d + se \quad (1)$$

In (1), $f(s)$ may denote an impedance-, admittance-, scattering-parameters function or a transfer function, obtained either analytically or from measurements; c_k and a_k are the residues and poles, respectively, they can be real or complex conjugate pairs; and d and e are real coefficients.

For multiport systems, $f(s)$ is a matrix function, which requires every element of it to be approximated as in (1). Matrix functions are usually fitted using a common set of poles for computational efficiency purposes [11]. For symmetrical matrix functions, such as the cases addressed in this paper, only the lower triangular part of the matrix is fitted. The rest of the elements are repeated according to symmetry.

The fitted model, as shown at the right hand side of (1) can be finally arranged as a state-space model for transient simulations [12]. A common characteristic of the studied techniques is that during the fitting process unstable poles may appear, which in turn, are corrected or removed to ensure stability of models.

A. Vector Fitting

The VF technique first computes the poles of (1) in an iterative relocation process from an initial (guessed) set of poles. For this purpose, VF introduces the auxiliary function

$$\sigma(s) = \sum_{k=1}^N \frac{\tilde{c}_k}{s - a_k} + 1 \quad (2)$$

to create the augmented problem

$$\sum_{k=1}^N \frac{c_k}{s - a_k} + d + se = \left(\sum_{k=1}^N \frac{\tilde{c}_k}{s - a_k} + 1 \right) f(s). \quad (3)$$

As it can be observed from (2), $\sigma(s)$ contains the same set of poles as $f(s)$, but different residues. Evaluating (3) for a predefined frequency band, the overdetermined set of equations

$$\mathbf{A}\mathbf{x} = \mathbf{b} \quad (4)$$

is obtained, where, the k th row of \mathbf{A} and \mathbf{x} are denoted by

$$\left[\frac{1}{s_k - a_1} \quad \cdots \quad \frac{1}{s_k - a_N} \quad 1 \quad s_k \quad \frac{-f(s_k)}{s_k - a_1} \quad \cdots \quad \frac{-f(s_k)}{s_k - a_N} \right] \quad (5)$$

$$\mathbf{x} = [c_1 \quad \cdots \quad c_N \quad d \quad e \quad \tilde{c}_1 \quad \cdots \quad \tilde{c}_N]^T \quad (6)$$

and \mathbf{b} contains the samples of $f(s)$. Note that this formulation only stands for real poles. To consider complex poles, (5) and (6) are modified accordingly [3].

Solving the least-squares problem (4), the residues of $\sigma(s)$ are obtained. At this point, $\sigma(s)$ is completely identified, then, its zeros are computed. As it is demonstrated in [3], the zeros of $\sigma(s)$ can be set equal to the poles of the system, such that an improved set of poles is obtained. This process can be repeated for a predefined number of iterations or until reaching convergence.

The second stage of VF consists of the calculation of residues and coefficients d and e . To do so, a new least-squares problem is formulated based on (1) using the obtained poles. In this case, the k th row of \mathbf{A} and \mathbf{x} , are:

$$\mathbf{A}_k = [1/(s_k - a_1) \quad \cdots \quad 1/(s_k - a_N) \quad 1 \quad s_k] \quad (7)$$

$$\mathbf{x} = [c_1 \quad \cdots \quad c_N \quad d \quad e]^T. \quad (8)$$

A complementary analysis of VF can be found in [13].

B. Matrix Pencil Method

The original MPM technique consists of the identification of a system by approximating its transient response $y(t)$ in discrete form as a sum of complex exponentials [14], i.e.,

$$y(k\Delta t) = \sum_{n=1}^N c_n e^{a_n k \Delta t} \quad (9)$$

where c_n and a_n are the time-domain counterpart of the residues and poles in (1), respectively, according to the Laplace transform. MPM identifies the poles of the system by solving the generalized eigenvalue problem:

$$\mathbf{Y}_1 \mathbf{v} = \lambda \mathbf{Y}_2 \mathbf{v} \quad (10)$$

where \mathbf{v} is a generalized eigenvector and λ its corresponding eigenvalue; \mathbf{Y}_1 and \mathbf{Y}_2 are the pencil matrices, which contain the samples of the transient response $y(t)$, see [7] for details.

The n th exponential term $e^{a_n \Delta t}$ in (9) is related to the n th eigenvalue as follows

$$\lambda_n = e^{a_n \Delta t}. \quad (11)$$

Such that the poles (a_n) are readily obtained from the set of eigenvalues of the pencil function (10) by solving (11).

To obtain the appropriate fitting order, the pencil matrices are subjected to Singular Value Decomposition (SVD), i.e.,

$$\mathbf{Y}_1 = \mathbf{U}_1 \Sigma \mathbf{R}_1 \quad (12)$$

$$\mathbf{Y}_2 = \mathbf{U}_2 \Sigma \mathbf{R}_2 \quad (13)$$

Considering only the N dominant singular values z_i , contained in the diagonal matrix Σ in (12) or (13), the eigenvalue problem (10) can be equivalently solved as

$$\hat{\mathbf{R}}_1 \mathbf{v} = \lambda \hat{\mathbf{R}}_2 \mathbf{v} \quad (14)$$

where $\hat{\mathbf{R}}_1$ and $\hat{\mathbf{R}}_2$ contain only the N dominant right eigenvectors of \mathbf{R}_1 in (12) and \mathbf{R}_2 in (13), respectively [14].

To determine the function order N , the singular values are first normalized by the largest one (z_1) i.e.,

$$\bar{z}_i = z_i / z_1 \quad (15)$$

then, the normalized singular values with magnitudes above a predefined tolerance value ζ are considered as dominant. Alternatively, if the function order is known, the first N singular values can be selected directly.

For noisy transient responses, the total-least-squares Matrix Pencil \mathbf{M} can be used instead of \mathbf{Y}_1 and \mathbf{Y}_2 . Like \mathbf{Y}_1 and \mathbf{Y}_2 , \mathbf{M} is computed using the samples of $y(t)$ as shown in [14]. Using \mathbf{M} , the corresponding SVD becomes:

$$\mathbf{M} = \mathbf{U} \Sigma \mathbf{R}, \quad (16)$$

and the pencil eigenvalues are calculated solving (14) with

$$\hat{\mathbf{R}}_1 = [\mathbf{r}_1 \quad \mathbf{r}_2 \quad \cdots \quad \mathbf{r}_{N-1}], \quad (17)$$

$$\hat{\mathbf{R}}_2 = [\mathbf{r}_2 \quad \mathbf{r}_3 \quad \cdots \quad \mathbf{r}_N], \quad (18)$$

where $\mathbf{r}_{1,2,\dots,N}$ denote the dominant right eigenvectors (columns of \mathbf{R}) obtained from (16). This approach is used in this paper.

Once the poles a_n are known, the residues c_n and coefficients d and e are calculated solving (7) and (8), similar to the VF technique.

Since the MPM technique described uses a transient response as input, the frequency-domain application requires a transformation to the time-domain [6, 7]. This transformation delimits the frequency-domain fitting to only linearly-spaced sampled functions. In this paper, transformation to time-domain is performed via the built-in Matlab function *IFFT* [6].

For matrix functions, the described MPM technique can be applied to each element of it, however, to obtain a common set of poles, the trace of the matrix is used in this paper.

C. Loewner Matrix fitting technique

The LM fitting technique uses tangential interpolation data to construct the state-space model:

$$\mathbf{Q} \dot{\mathbf{x}}(t) = \mathbf{A} \mathbf{x}(t) + \mathbf{B} \mathbf{u}(t) \quad (19)$$

$$\mathbf{y}(t) = \mathbf{C} \mathbf{x}(t) + \mathbf{D} \mathbf{u}(t) + \mathbf{Y}^\infty \dot{\mathbf{u}}(t) \quad (20)$$

where \mathbf{Q} , $\mathbf{A} \in \mathbb{R}^{m \times m}$, $\mathbf{B} \in \mathbb{R}^{m \times p}$, $\mathbf{C} \in \mathbb{R}^{p \times m}$, $\mathbf{x} \in \mathbb{R}^{m \times 1}$, $\mathbf{y} \in \mathbb{R}^{p \times 1}$, \mathbf{D} , $\mathbf{Y}^\infty \in \mathbb{R}^{p \times p}$, with p being the number of inputs/outputs and m the number of states. This state-space model is obtained by first applying SVD to the Loewner pencil function as follows:

$$\Lambda \Sigma \Psi = \text{SVD}(x\mathbf{L} - \mathbf{L}') \quad (21)$$

where x can be any sample of $s = j\omega$ that is not an eigenvalue of the pencil function, and \mathbf{L} and \mathbf{L}' denote the Loewner and shifted-Loewner matrices, respectively. These matrices are computed as follows:

$$\mathbf{L}_{ij} = (\Phi_j \mathbf{r}_i - \mathbf{I}_j \Omega_i) / (\mu_j - \lambda_i) \quad (22)$$

$$\mathbf{L}'_{ij} = (\mu_j \Phi_j \mathbf{r}_i - \lambda_i \mathbf{I}_j \Omega_i) / (\mu_j - \lambda_i) \quad (23)$$

where $\{\mu_j, \mathbf{I}_j$ and $\Phi_j\}$ and $\{\lambda_i, \mathbf{r}_i$ and $\Omega_i\}$ denote the left and right tangential interpolation data, respectively.

Tangential interpolation data is constructed as follows:

$$\mu = [s_1 \quad s_1^* \quad s_3 \quad s_3^* \quad \cdots \quad s_{N_s-1} \quad s_{N_s-1}^*] \quad (24)$$

$$\lambda = [s_2 \quad s_2^* \quad s_4 \quad s_4^* \quad \cdots \quad s_{N_s} \quad s_{N_s}^*] \quad (25)$$

$$\Phi_j = \mathbf{I}_j \mathbf{F}(\mu_j) \quad (26)$$

$$\Omega_i = \mathbf{F}(\lambda_i) \mathbf{r}_i \quad (27)$$

$$\mathbf{P} = [\Phi_1^T \quad \cdots \quad \Phi_j^T \quad \cdots]^T \quad (28)$$

$$\mathbf{W} = [\Omega_1 \quad \cdots \quad \Omega_i \quad \cdots] \quad (29)$$

From (26) and (27), \mathbf{F} denotes the matrix function being fitted; \mathbf{l}_j and \mathbf{r}_i are referred as left and right tangential directions, respectively, and they can be VFTI (vector-format tangential interpolation) or MFTI (matrix-format tangential interpolation) type [9], being the last one used in this paper.

Finally, the state-space model (19)-(20) is computed as:

$$\mathbf{Q} = -\Lambda_r^* \mathbf{L} \Psi_r \quad (30)$$

$$\mathbf{A} = -\Lambda_r^* \mathbf{L}' \Psi_r \quad (31)$$

$$\mathbf{B} = \Lambda_r^* \mathbf{P}_r \quad (32)$$

$$\mathbf{C} = \mathbf{W}_r \Psi_r \quad (33)$$

where the subscript r means that only the columns related to the dominant singular values revealed in (21) are used for each matrix. The dominant singular values in (21) are selected as explained in the previous section. The number of dominant singular values equals the number of states in (19)-(20).

At this stage, \mathbf{D} and \mathbf{Y}^∞ in (20) are embedded into the model described by (30)-(33), however, since \mathbf{Y}^∞ contains unstable modes, it must be extracted. Different strategies have been proposed to do so [8, 9, 15], however, this paper proposes a novel approach for extraction of \mathbf{Y}^∞ as follows. The built-in Matlab function $pole(sys)$ is used to extract the poles to the model given by (30)-(33), the resulted unstable poles are removed (equivalent to the extraction of \mathbf{Y}^∞). Finally, using the extracted (stable) poles, residues and d and e coefficients are calculated solving (7) and (8) via least squares, like the VF technique. This approach allows a fair comparison of LM with VF and MPM techniques.

III. NUMERICAL EXAMPLES

In this section, VF, MPM and LM techniques are compared by fitting different frequency-domain functions. In all cases, VF is applied with six iterations and no weighting schemes are used. To evaluate the fittings, two metrics are used, i.e., the RMS error ε_{RMS} and the relative error $\varepsilon_{relative}$, computed as follows:

$$\varepsilon_{RMS} = \sqrt{\sum_{k=1}^{N_s} \sum_{n=1}^{N_e} |\mathbf{f}_n(s_k) - \mathbf{f}'_n(s_k)|^2 / (N_s N_e)} \quad (34)$$

$$\varepsilon_{relative} = \sum_{k=1}^{N_s} \sum_{n=1}^{N_e} \left[\frac{|\mathbf{f}_n(s_k) - \mathbf{f}'_n(s_k)|}{|\mathbf{f}_n(s_k)|} \times 100 \right] / (N_s N_e) \quad (35)$$

where \mathbf{f} is a vector containing the elements of the lower triangular part of the matrix function fitted, these elements are stacked to form a single column, N_e denotes the number of elements of \mathbf{f} ; N_s denotes the number of frequency samples; and \mathbf{f}' denotes the frequency response of the fitted model.

A. Low-order synthetic function

The fitting of the frequency-domain function (36) is performed using VF, MPM and LM techniques. The function is evaluated from 0 to 1 kHz with 200 linearly spaced samples.

$$f(s) = \frac{2}{s+5} + \frac{30 \pm j40}{s+100 \pm j500} + 0.5 \quad (36)$$

As a first test, the correct order of the function $N = 3$ and non-zero d coefficient are set for the three techniques. The

resultant fitting magnitude curves are shown in Fig. 1. The function coefficients obtained via VF technique are the same as those of (36), while the coefficients obtained via MPM and LM techniques, presented in (37) and (38), are considerably different. Thus, based on both, fitting curves and function coefficients, it can be said that VF performs the best fitting for this case.

$$f_{MPM}(s) = \frac{25}{s+2641} + \frac{34 \pm j77}{s+259 \pm j385} + 0.496 \quad (37)$$

$$f_{LM}(s) = \frac{7 \times 10^5}{s+2 \times 10^6} + \frac{29 \pm j36}{s+93 \pm j506} + 0.14 \quad (38)$$

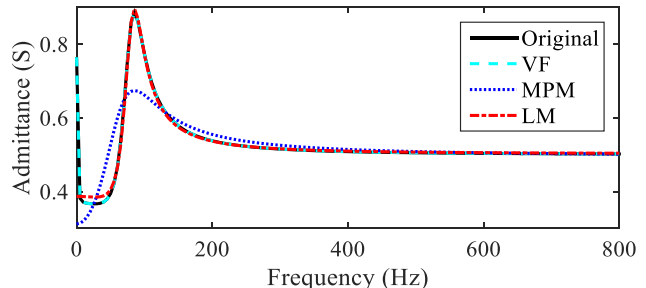


Fig. 1. Magnitude of the synthetic function (36) fitted with $N = 3$.

The singular values of the LM pencil show a clear drop at the fourth singular value, revealing the order of the system (including the d coefficient) as reported in [9]; on the other hand, the singular values of the MPM pencil function draw a smooth curve, which makes more difficult the order identification. Both cases are shown in Fig. 2.

Setting for example $\zeta = 1 \times 10^{-5}$ for model order identification (marked by the horizontal dashed-line in Fig. 2), MPM fitting is very accurate, but the model order is increased; on the other hand, LM fitting becomes less accurate. These results are summarized in Table I, where the RMS and relative error for each case are presented.

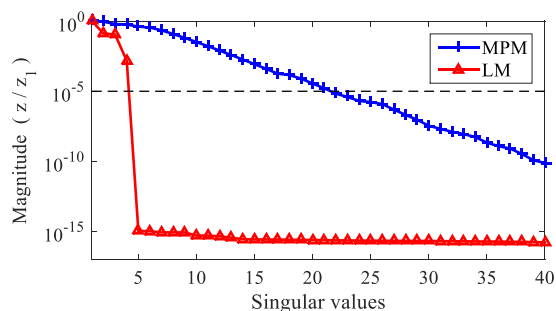


Fig. 2. Pencil singular values of synthetic function (36).

TABLE I.
COMPARISON OF FITTING ACCURACY OF VF, MPM AND LM FOR FITTING THE SYNTHETIC FUNCTION (36).

Technique	Order	ζ	ε_{RMS}	$\varepsilon_{relative}$
VF	3	-	9.52×10^{-16}	$1.76 \times 10^{-13} \%$
	3	-	6.15×10^{-2}	4.85 %
MPM	21	1×10^{-5}	8.69×10^{-7}	$8.65 \times 10^{-5} \%$
	3	-	1.98×10^{-2}	0.61 %
LM	4	1×10^{-5}	0.13	12.48 %

B. Transformer

The fitting of the zero-sequence admittance of the 11kV/230V transformer adopted from [3] is achieved. Both MPM and LM pencil singular values, plotted in Fig. 3, show a large drop at the sixth eigenvalue, revealing the model order. Using $N = 6$, the fitting magnitude plot obtained is shown in Fig. 4. This figure shows that VF and LM achieve very accurate fittings while MPM fitting is poorer. The corresponding RMS and relative fitting errors, given in Table II, show that LM is the most accurate technique for this case.

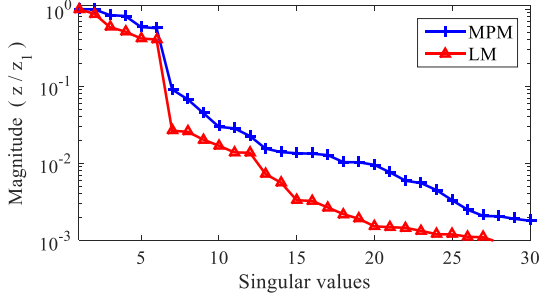


Fig. 3. MPM and LM pencil singular values of transformer case study.

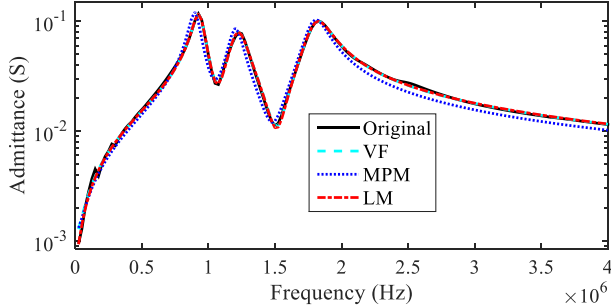


Fig. 4. Magnitude fitting plot of transformer case study.

TABLE II.
COMPARISON OF FITTING TECHNIQUES FOR TRANSFORMER ADMITTANCE CASE STUDY USING 6 POLES.

Technique	\mathcal{E}_{RMS}	$\mathcal{E}_{relative}$
VF	1.17×10^{-3}	6.32 %
MPM	8.68×10^{-3}	24.68 %
LM	1.09×10^{-3}	4.89 %

C. PI circuit

The admittance matrix of the circuit of Fig. 5, seen from nodes 1 and 2, is fitted using the studied techniques. The admittances Y_a , Y_b and Y_c , are given in (39), (40), and (41), respectively. Since these admittances contain a total of nine partial fractions, the optimal fitting order is $N = 9$. The LM pencil singular values, plotted in Fig. 6, show a large drop at the 11th singular value (close to the correct order), while the MPM singular values, shown in the same figure, draw a smooth curve.

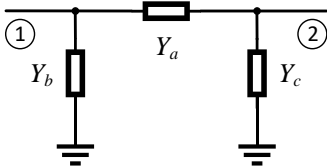


Fig. 5. PI circuit case study.

$$Y_a(s) = \frac{2}{s+5} + \frac{20 \pm j50}{s+30 \pm j1000} + 0.4, \quad (39)$$

$$Y_b(s) = \frac{6}{s+12} + \frac{17 \pm j30}{s+35 \pm j3000} + 0.2, \quad (40)$$

$$Y_c(s) = \frac{4}{s+10} + \frac{12 \pm j24}{s+15 \pm j5500} + 0.3. \quad (41)$$

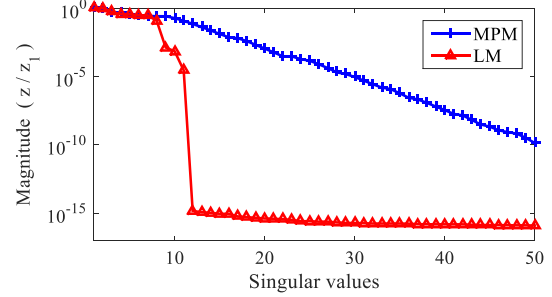


Fig. 6. Pencil singular values of 2×2 admittance matrix of circuit of Fig. 5.

Setting $N = 9$ and non-zero \mathbf{D} matrix for the fitting of the admittance matrix of the circuit of Fig. 5, the magnitude plots shown in Fig. 7 (a), (b) and (c) are obtained. From Fig. 7 (a), it can be observed that only MPM technique achieves a poor fitting for element $\mathbf{Y}(1,1)$ around 440 Hz. The rest of elements are accurately fitted for every technique.

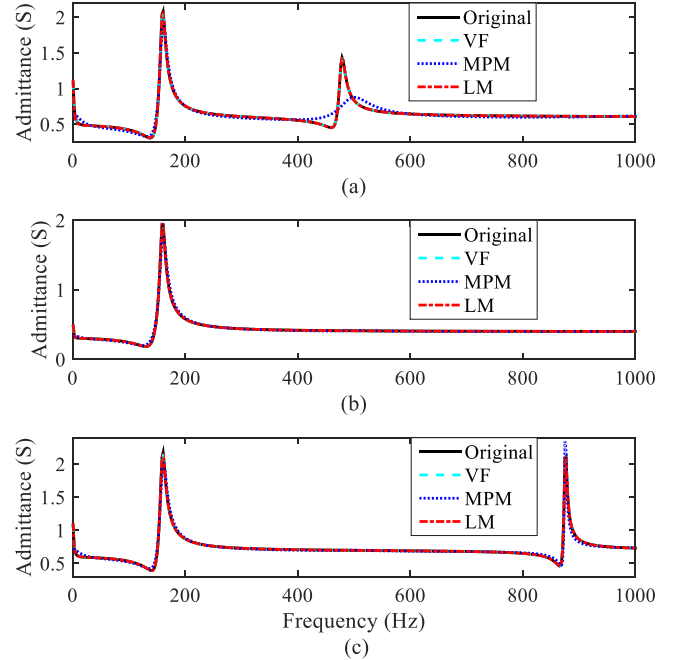


Fig. 7. Fitting magnitude plots of 2×2 admittance matrix with 9 poles. (a) Element $\mathbf{Y}(1,1)$, (b) Element $\mathbf{Y}(1,2)$, (c) Element $\mathbf{Y}(2,2)$.

To further assess the performance of the studied fitting techniques, the fitting is repeated using $N = 6$ and $N = 12$. The resulting fitting magnitude plots of element $\mathbf{Y}(1,1)$ are shown in Fig. 8 (a) and (b). Fig. 8 (a) shows that when the system order is underestimated, fitting accuracy is similar (poor) for the three techniques; however, when fitting order is overestimated, Fig. 8 (b), only LM fitting loses accuracy (as occurred for the synthetic function example presented before).

The RMS and relative errors for the different orders tested are listed in Table III. This table confirms that the VF technique achieves the most accurate fittings in all cases.

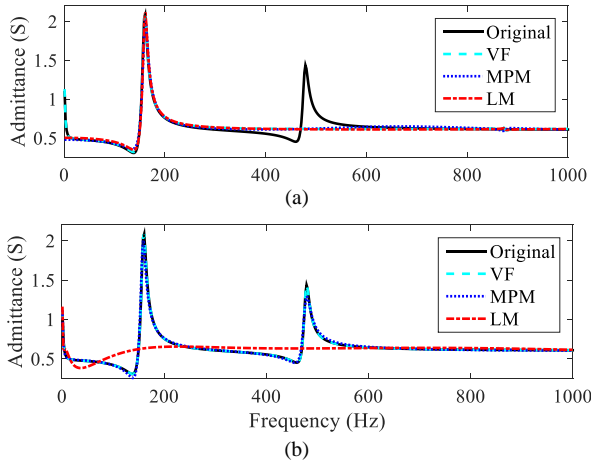


Fig. 8. Magnitude plot of $Y(1,1)$ of pi circuit case study, (a) $N=6$, (b) $N=12$.

TABLE III.
COMPARISON OF FITTING TECHNIQUES FOR PI CIRCUIT CASE STUDY.

Technique	Order	\mathcal{E}_{RMS}	$\mathcal{E}_{relative}$
VF		6.7×10^{-2}	2.64 %
MPM	6	8.5×10^{-2}	4.92 %
LM		7.5×10^{-2}	3.73 %
VF		5.10×10^{-15}	2.69×10^{-13} %
MPM	9	6.38×10^{-2}	4.12 %
LM		2.22×10^{-3}	8.6×10^{-2} %
VF		2×10^{-14}	6.53×10^{-13} %
MPM	12	3.1×10^{-2}	2.22 %
LM		0.21	13.93 %

D. Distribution Network FDNE

A more challenging case study, such as fitting an FDNE for the distribution network of Fig. 9 (adopted from [16]) is studied in this section. The magnitudes of the elements of the admittance matrix of the system measured from nodes **A** and **B** are plotted in Fig. 10. Since the system order cannot be determined by simple inspection, MPM and LM techniques are used to determine the system order. From Fig. 11, it can be observed that neither the LM nor the MPM pencil singular values exhibit any large drops. Then, N should be determined by appropriate selection of ζ .

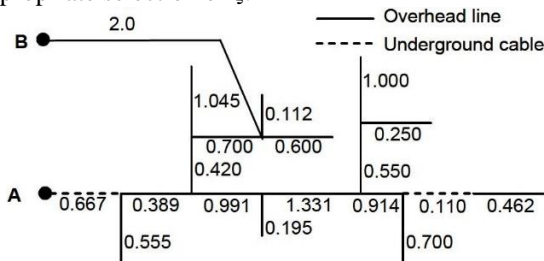


Fig. 9. Distribution network case study.

To analyze the impact of ζ , Fig. 12 shows the resulting RMS errors for different values of ζ . This figure shows that the RMS error by MPM fitting converges to a certain limit as ζ

tends to zero, whereas the RMS error obtained with LM varies almost linearly with ζ . This fact suggests that LM technique has better control of fitting accuracy.

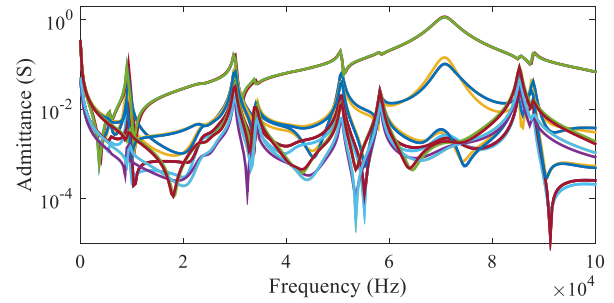


Fig. 10. Magnitude of the elements of the admittance matrix of the distribution network of Fig. 9.

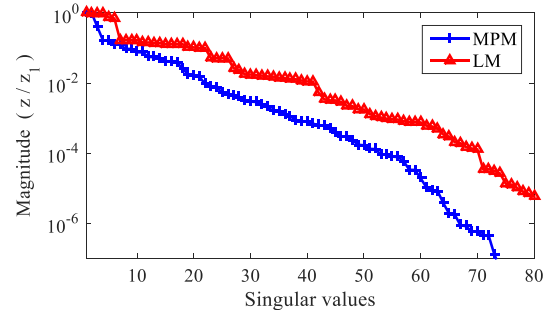


Fig. 11. Singular values of the MPM and LM pencils of the distribution network case study.

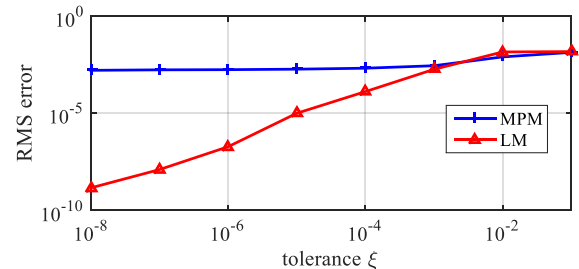


Fig. 12. Illustration of the impact of ζ over fitting accuracy for MPM and LM techniques for the distribution network case study.

From this example, it is also observed that reducing the tolerance value ζ (to improve fitting accuracy) in MPM and LM techniques, can considerably increase the model order N , which is desired to be as low as possible for better computational performance in transient simulations. A plot of the order N versus the relative error for the studied fitting techniques is presented in Fig. 13. This figure reveals that for any given order, the VF technique is the most accurate.

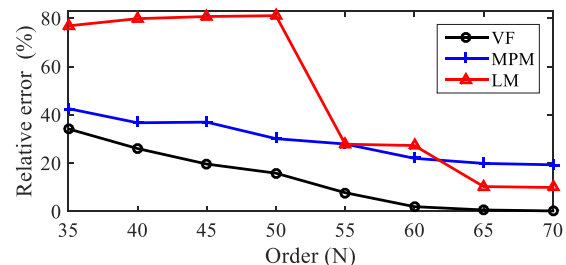


Fig. 13. Relative error relationship respect to fitting order for the distribution system FDNE case study.

E. Transmission cable system

As final case study, the transmission cable system presented in [17], is used for the computation of an equivalent transient model. The admittance matrix elements measured from sending and receiving terminals are plotted in Fig. 14. The number of frequency points measured is 2500. The fitting results using an order of $N = 50$ are summarized in Table IV. As in most previous examples, VF obtains the lowest error. This table also reveals a disadvantage of MPM and LM techniques, i.e., the CPU time required can be considerably long when the number of frequency samples is substantial.

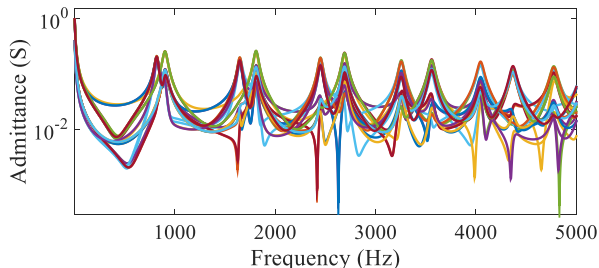


Fig. 14. Elements of the admittance matrix of the transmission cable studied.

TABLE IV.
COMPARISON OF FITTING TECHNIQUES FOR CABLE SYSTEM CASE STUDY.

Technique	\mathcal{E}_{RMS}	$\mathcal{E}_{relative}$	CPU
VF	1.40×10^{-5}	$6.6 \times 10^{-2} \%$	6.5 s
MPM	1.71×10^{-3}	2.53 %	473 s
LM	2.08×10^{-3}	1.27 %	1847 s

IV. DISCUSSION

The main observation of the examples presented is that for any given fitting order, VF achieves the most accurate fittings among the studied techniques.

It has also been verified that the accuracy of MPM and LM techniques can be as good as VF but at the cost of increasing the model order, which is undesirable for model efficiency in time-domain simulations. From this observation, one more important fact can be established, i.e., the fitted models obtained using MPM and LM are not minimal representations, since there always exists another system representation with same accuracy level but lower order, as given by VF (this does not mean that VF gives minimal representations either).

A unique advantage of MPM and LM is that they provide the order identification as dictated by the singular values of corresponding pencils; however, the drop in the singular values is not always evident. Then, fitting accuracy must be tuned by appropriate selection of the tolerance value ζ .

For low-order models, such as the presented synthetic function and transformer examples, LM singular values show clear drops, which allows an easy order identification, while for highly resonant admittance functions such as the FDNEs and the transmission cable system presented, both MPM and LM singular values draw smooth curves.

Finally, a poor performance in terms of CPU time has been observed for MPM and LM techniques when the function to fit has substantial number of points, such as the studied transmission cable system.

V. CONCLUSIONS

This paper presents a comparison of VF, MPM, and LM fitting techniques through the fitting of different frequency-domain functions. The studied test cases demonstrate that VF achieves the best tradeoff between fitting accuracy and model order. Nonetheless, MPM and LM techniques are useful for model order identification, especially for low-order models. Then, for those cases, the model order obtained via MPM or LM can be used as an input to the VF technique.

VI. REFERENCES

- [1] B. Gustavsen and A. Semlyen, "Simulation of transmission line transients using vector fitting and modal decomposition," *IEEE Transactions on Power Delivery*, vol. 13, pp. 605-614, Apr 1998.
- [2] B. Gustavsen and A. Semlyen, "Application of vector fitting to state equation representation of transformers for simulation of electromagnetic transients," *IEEE Transactions on Power Delivery*, vol. 13, pp. 834-842, Jul 1998.
- [3] B. Gustavsen and A. Semlyen, "Rational approximation of frequency domain responses by vector fitting," *IEEE Transactions on Power Delivery*, vol. 14, pp. 1052-1061, Jul 1999.
- [4] D. Deschrijver, M. Mrozowski, T. Dhaene, and D. De Zutter, "Macromodeling of Multiport Systems Using a Fast Implementation of the Vector Fitting Method," *IEEE Microwave and Wireless Components Letters*, vol. 18, pp. 383-385, 2008.
- [5] B. Gustavsen, "Improving the pole relocating properties of vector fitting," *IEEE Transactions on Power Delivery*, vol. 21, pp. 1587-1592, Jul 2006.
- [6] K. Sheshyekani and B. Tabei, "Multiport Frequency-Dependent Network Equivalent Using a Modified Matrix Pencil Method," *IEEE Transactions on Power Delivery*, vol. 29, pp. 2340-2348, Oct 2014.
- [7] K. Sheshyekani, H. R. Karami, P. Dehkhoda, M. Paolone, and F. Rachidi, "Application of the Matrix Pencil Method to Rational Fitting of Frequency-Domain Responses," *IEEE Transactions on Power Delivery*, vol. 27, pp. 2399-2408, Oct 2012.
- [8] G. Gurrara, "Loewner matrix approach for modelling FDNEs of power systems," *Electric Power Systems Research*, vol. 125, pp. 116-123, Aug 2015.
- [9] M. Kabir and R. Khazaka, "Macromodeling of Distributed Networks From Frequency-Domain Data Using the Loewner Matrix Approach," *IEEE Transactions on Microwave Theory and Techniques*, vol. 60, pp. 3927-3938, Dec 2012.
- [10] S. Lefteriü and A. C. Antoulas, "A New Approach to Modeling Multiport Systems From Frequency-Domain Data," *IEEE Transactions on Computer-Aided Design of Integrated Circuits and Systems*, vol. 29, pp. 14-27, 2010.
- [11] B. Gustavsen, "Computer code for rational approximation of frequency dependent admittance matrices," *IEEE Transactions on Power Delivery*, vol. 17, pp. 1093-1098, 2002.
- [12] B. Gustavsen and A. Semlyen, "A robust approach for system identification in the frequency domain," *IEEE Transactions on Power Delivery*, vol. 19, pp. 1167-1173, Jul 2004.
- [13] I. Kocar, J. Mahseredjian, and G. Olivier, "Weighting method for transient analysis of underground cables," *IEEE Transactions on Power Delivery*, vol. 23, pp. 1629-1635, Jul 2008.
- [14] T. K. Sarkar and O. Pereira, "Using the Matrix Pencil Method to Estimate the Parameters of a Sum of Complex Exponentials," *IEEE Antennas and Propagation Magazine*, vol. 37, pp. 48-55, Feb 1995.
- [15] M. Kabir and R. Khazaka, "Loewner Matrix Macromodeling for Y-Parameter Data With a Priori D Matrix Extraction," *IEEE Transactions on Microwave Theory and Techniques*, vol. 64, pp. 4098-4107, Dec 2016.
- [16] D. Deschrijver, B. Gustavsen, and T. Dhaene, "Advancements in iterative methods for rational approximation in the frequency domain," *IEEE Transactions on Power Delivery*, vol. 22, pp. 1633-1642, Jul 2007.
- [17] I. Lafaia, J. Mahseredjian, A. Ametani, M. T. Correia de Barros, and I. Koçar, "Frequency and Time Domain Responses of Cross-Bonded Cables," *IEEE Transactions on Power Delivery*, 2017.